Quantum extension of the Vlasov method

S. J. Lee*
Physics Department, McGill University, Montreal, Quebec, Canada H3A 2T8
(Received 18 September 1989)

The quantum correction to the Vlasov equation is considered using the Wigner transform of the time-dependent Hartree-Fock equation without truncation in $\hbar$ order. Decomposing the Wigner function in terms of test particles with the form factor in a phase space, quantum extension of the Vlasov equation determines the equation of motion of the test particle which follows classical dynamics. The discrimination between the quantum and classical limits is related to a density matrix condition which constrains the distribution of test particles.

I. INTRODUCTION

The time-dependent Hartree-Fock (TDHF) approximation has been used extensively in the past to analyze heavy-ion collisions at low to moderate energies. However, at higher energies, we should consider collision terms which have been neglected in TDHF. In extended TDHF, two-body collisions are incorporated through a time-dependent density matrix (TDDM) (Refs. 1, 2, and 3) with TDHF mean-field propagation. There is difficulty in describing intermediate energy collisions which is related to the fact that TDHF is described in a configuration space and that the nucleon-nucleon collision induces abrupt momentum change of the nucleon involved in intermediate energy collisions. The time-dependent Vlasov equation, which is described in a phase space, can be derived as a semiclassical approximation to the TDHF equation. In TDHF, the single nucleon orbitals ψ_α evolve according to

$$i\hbar\frac{\partial\psi_\alpha}{\partial t}=(T+U)\psi_\alpha \ . \tag{1}$$

Here the wave function of the system, which should be antisymmetric due to the Pauli principle, is represented by a single Slater determinant built with occupied single nucleon orbitals. In a Slater determinant, the density matrix has the property of projection operator, i.e.,

$$\rho^2=\rho \ , \tag{2}$$

and the one-body density matrix evolves according to, from Eq. (1),

$$i\hbar\frac{\partial\rho}{\partial t}=[H,\rho] \ . \tag{3}$$

Here $H=T+U$ is the TDHF single particle mean-field Hamiltonian.

Defining the Wigner transformation of an operator O

$$\begin{aligned}O_\sigma^{\sigma'}(\mathbf{r},\mathbf{p})&=\int d^3s e^{-i\mathbf{p}\cdot\mathbf{s}/\hbar}\langle \mathbf{r}+\mathbf{s}/2,\sigma|O|\mathbf{r}-\mathbf{s}/2,\sigma'\rangle \\ &=\int d^3r_1 d^3r_2 e^{-i\mathbf{p}\cdot(\mathbf{r}_1-\mathbf{r}_2)/\hbar}\langle \mathbf{r}_1,\sigma|O|\mathbf{r}_2,\sigma'\rangle \\ &\quad\times\delta\left[\mathbf{r}-\frac{\mathbf{r}_1+\mathbf{r}_2}{2}\right] ,\end{aligned} \tag{4}$$

where σ represents the spin-isospin quantum number, then a Wigner transform of density matrix ρ,

$$\rho(\mathbf{r},\mathbf{r}',t)=\sum_\sigma\langle \mathbf{r},\sigma|\rho|\mathbf{r}',\sigma\rangle=\sum_\alpha\psi_\alpha^*(\mathbf{r},t)\psi_\alpha(\mathbf{r}',t) \ , \tag{5}$$

becomes

$$4\tilde{f}(\mathbf{r},\mathbf{p},t)=\int d^3s e^{-i\mathbf{p}\cdot\mathbf{s}/\hbar}\rho(\mathbf{r}+\mathbf{s}/2,\mathbf{r}-\mathbf{s}/2,t) \ . \tag{6}$$

Here the factor of 4 is used to represent the spin-isospin degeneracy and the single nucleon orbital index α represents all the quantum numbers including the spin-isospin quantum number σ. The phase space density $f(\mathbf{r},\mathbf{p},t)$, which is called the Wigner function, can be defined as

$$\begin{aligned}f(\mathbf{r},\mathbf{p},t)&=\frac{4}{(2\pi\hbar)^3}\tilde{f}(\mathbf{r},\mathbf{p},t) \\ &=\frac{1}{(2\pi\hbar)^3}\int d^3s\, e^{-i\mathbf{p}\cdot\mathbf{s}/\hbar}\rho(\mathbf{r}+\mathbf{s}/2,\mathbf{r}-\mathbf{s}/2,t) \ .\end{aligned} \tag{7}$$

Notice here that the Wigner function f (or equivalently $\tilde{f}$) can become negative at some region in the six-dimensional phase space. In a classical limit, i.e., $\hbar\to 0$ limit, a Wigner transformation of the density matrix condition, Eq. (2), gives the condition on $\tilde{f}(\mathbf{r},\mathbf{p},t)$ as

$$\tilde{f}^2=\tilde{f} \ . \tag{8}$$

Due to this condition the Wigner function in a classical limit cannot have a negative value and thus becomes a semiclassical distribution function; $\tilde{f}$ can be only 1 or 0 due to the condition of Eq. (8). A Wigner transformation of the TDHF equation (3), in a classical limit, gives a time-dependent Vlasov equation for the time evolution of the Wigner function $f(\mathbf{r},\mathbf{p},t)$ as

$$\frac{\partial}{\partial t}f(\mathbf{r},\mathbf{p},t)+[\nabla_p H(\mathbf{r},\mathbf{p})]\cdot\nabla f(\mathbf{r},\mathbf{p},t)-[\nabla H(\mathbf{r},\mathbf{p})]\cdot\nabla_p f(\mathbf{r},\mathbf{p},t)=0\ , \tag{9}$$

where ∇ and ∇_p mean the gradients in r and p space, respectively, and

$$H(\mathbf{r},\mathbf{p})=\frac{p^2}{2m^*}+U(\mathbf{r},\mathbf{p}) \tag{10}$$

is the Wigner transform of the TDHF mean-field Hamiltonian $H=T+U$ with an effective mass m^*.

Using the phase space density $f(\mathbf{r},\mathbf{p},t)$, it becomes clear how to incorporate the mean-field propagation with collision terms. The time-dependent Vlasov equation, replacing the right-hand side of Eq. (9) by the Boltzmann-Uehling-Uhlenbeck (BUU) collision integral, has been used extensively in the past to analyze heavy-ion collisions at intermediate energies (details can be found in Ref. 4). One of the problems with the Vlasov prescription is related to the classical approximation. Therefore, quantum effects have been neglected in the Vlasov method except for the approximate inclusion of the Pauli principle through Eq. (8). For a static nucleus, the self-consistent density in Vlasov method with a momentum-independent local mean-field potential has a sharp surface[5,6] in contrast to the TDHF case in which the density ty has a long tail. Quantum extension of the Vlasov prescription has been sought for a long time. Gregoire *et al.*[7] have obtained a diffuse surface by mapping the phase space density with Gaussian packets in the classical Vlasov equation with a local mean-field potential. Their one-dimensional slab calculations show that there are very close similarities with TDHF. They have not considered higher-order terms in $\hbar$ and claimed that the diffuse surface comes from mocking up the quantum effects through Gaussians with finite width. Kohl, Schuck, and Stringari[8] have considered higher-order corrections in $\hbar$ analytically for a spherical harmonic oscillator with separable quadrupole-quadrupole and octupole-octupole time-dependent interactions. Since underlying time-dependent forces are separable and are not self-consistent, the quadrupole mode in this model has no quantum correction and the octupole mode has only second-order correction in $\hbar$.

The purpose of this paper is the systematic quantum extension of the Vlasov equation, Eq. (9), starting from the exact Wigner transform of the TDHF equation (3). Full Wigner transform of TDHF, which is a representation of TDHF in phase space, and its general properties are summarized in Sec. II. In Sec. III the so-called test particle method is discussed to solve the phase space representation of TDHF. Numerical solutions for a nucleus using this quantum extension of the Vlasov prescription are compared with the TDHF solutions in Sec. IV. Conclusions are presented in Sec. V.

II. WIGNER TRANSFORM OF TDHF AND ITS INVERSE TRANSFORMS

Defining the Wigner transformation of an operator as in Eq. (4), a Wigner transform of a product OQ of operators O and Q follows[9]

$$\begin{aligned}(O_\sigma^{\sigma''}Q_{\sigma''}^{\sigma'})(\mathbf{r},\mathbf{p})&=O_\sigma^{\sigma''}(\mathbf{r},\mathbf{p})e^{i(\hbar/2)(\overleftarrow{\nabla}\cdot\vec{\nabla}_p-\overleftarrow{\nabla}_p\cdot\vec{\nabla})}Q_{\sigma''}^{\sigma'}(\mathbf{r},\mathbf{p})\\&=Q_{\sigma''}^{\sigma'}(\mathbf{r},\mathbf{p})e^{-i(\hbar/2)(\overleftarrow{\nabla}\cdot\vec{\nabla}_p-\overleftarrow{\nabla}_p\cdot\vec{\nabla})}O_\sigma^{\sigma''}(\mathbf{r},\mathbf{p})\ ,\end{aligned} \tag{11}$$

where the direction of arrows over the gradients means the gradients act to the quantities on that side of the gradient. Using Wigner transformations, Eqs. (4) and (11), a full Wigner transform of the TDHF equation [Eq. (3)] becomes[9]

$$\frac{\partial}{\partial t}f(\mathbf{r},\mathbf{p},t)+\frac{2}{\hbar}f(\mathbf{r},\mathbf{p},t)\sin\left[\frac{\hbar}{2}(\overleftarrow{\nabla}\cdot\vec{\nabla}_p-\overleftarrow{\nabla}_p\cdot\vec{\nabla})\right]H(\mathbf{r},\mathbf{p})=0\ . \tag{12}$$

This is a representation of the TDHF equation in a phase space. Through the expansion of the sine function, Eq. (12) can be rewritten as

$$\frac{\partial}{\partial t}f(\mathbf{r},\mathbf{p},t)+[\nabla_p H(\mathbf{r},\mathbf{p})]\cdot\nabla f(\mathbf{r},\mathbf{p},t)-[\nabla H(\mathbf{r},\mathbf{p})]\cdot\nabla_p f(\mathbf{r},\mathbf{p},t)$$
$$=\sum_{n=1}^{\infty}\frac{(-1)^n}{(2n+1)!}\left[\frac{\hbar}{2}\right]^{2n}H(\mathbf{r},\mathbf{p})(\overleftarrow{\nabla}\cdot\vec{\nabla}_p-\overleftarrow{\nabla}_p\cdot\vec{\nabla})^{2n+1}f(\mathbf{r},\mathbf{p},t)\ . \tag{13}$$

A full Wigner transform of the density matrix condition, Eq. (2), becomes

$$\tilde{f}(\mathbf{r},\mathbf{p},t)\cos\left[\frac{\hbar}{2}(\overleftarrow{\nabla}\cdot\vec{\nabla}_p-\overleftarrow{\nabla}_p\cdot\vec{\nabla})\right]\tilde{f}(\mathbf{r},\mathbf{p},t)=\tilde{f}(\mathbf{r},\mathbf{p},t)\ , \tag{14}$$

where we have considered the spin-isospin degeneracy factor. Through the expansion of the cosine function, Eq. (14) can be rewritten as

$$\begin{aligned}\tilde{f}(\mathbf{r},\mathbf{p},t)\tilde{f}(\mathbf{r},\mathbf{p},t)-\tilde{f}(\mathbf{r},\mathbf{p},t)&=-\sum_{n=1}^{\infty}\frac{(-1)^n}{(2n)!}\left[\frac{\hbar}{2}\right]^{2n}\\&\times\tilde{f}(\mathbf{r},\mathbf{p},t)(\overleftarrow{\nabla}\cdot\vec{\nabla}_p-\overleftarrow{\nabla}_p\cdot\vec{\nabla})^{2n}\tilde{f}(\mathbf{r},\mathbf{p},t)\ .\end{aligned} \tag{15}$$

A classical limit, i.e., $\hbar \to 0$ limit, of Eqs. (15) and (13) become Eqs. (8) and (9), respectively, as in the ordinary Vlasov prescription.

For the Wigner transformation of Eq. (4), the inverse Wigner transformation[9] can be written as

$$O_{\sigma}^{\sigma'}(\mathbf{r}_1,\mathbf{r}_2)=\langle \mathbf{r}_1,\sigma|O|\mathbf{r}_2,\sigma'\rangle = \frac{1}{(2\pi\hbar)^3}\int d^3p\, d^3r\, e^{i\mathbf{p}\cdot(\mathbf{r}_1-\mathbf{r}_2)/\hbar} O_{\sigma}^{\sigma'}(\mathbf{r},\mathbf{p}) \times \delta\left[\mathbf{r}-\frac{\mathbf{r}_1+\mathbf{r}_2}{2}\right] . \tag{16}$$

This can be easily shown using the first expression of Eq. (4). The inverse Wigner transform of the Wigner function $f(\mathbf{r},\mathbf{p},t)$ becomes, considering the $(2\pi\hbar)^3$ factor in Eq. (7), the r-space representation of the density matrix $\rho(\mathbf{r}_1,\mathbf{r}_2)$ at t. For the $\mathbf{r}_1=\mathbf{r}_2=\mathbf{r}$ case, Eq. (16) becomes

$$O_{\sigma}^{\sigma'}(\mathbf{r})=\langle \mathbf{r},\sigma|O|\mathbf{r},\sigma'\rangle = \frac{1}{(2\pi\hbar)^3}\int d^3p\, O_{\sigma}^{\sigma'}(\mathbf{r},\mathbf{p}) . \tag{17}$$

Thus the integral over the p space of the Wigner transform of an operator O gives the diagonal element of O in the coordinate r-space representation. Specifically, we get

$$\rho(\mathbf{r},t)=\int d^3p f(\mathbf{r},\mathbf{p},t) . \tag{18}$$

The inverse Wigner transform of Eq. (14) becomes

$$\int d^3r_1 \rho(\mathbf{r},\mathbf{r}_1)\rho(\mathbf{r}_1,\mathbf{r}')=\rho(\mathbf{r},\mathbf{r}') . \tag{19}$$

This is the r-space representation of the density matrix condition Eq. (2). Similarly, the inverse Wigner transform of Eq. (12) gives the r-space representation of the TDHF equation (3) and the integral over p space of Eq. (12), specifically, gives the time evolution of the local density $\rho(\mathbf{r})$.

Now consider the integral over r space of the Wigner transformation Eq. (4). From the second expression,

$$\frac{1}{(2\pi\hbar)^3}\int d^3r O_{\sigma}^{\sigma'}(\mathbf{r},\mathbf{p})=\frac{1}{(2\pi\hbar)^3}\int d^3r_1 d^3r_2 e^{-i\mathbf{p}\cdot\mathbf{r}_1/\hbar}\langle \mathbf{r}_1,\sigma|O|\mathbf{r}_2,\sigma'\rangle e^{i\mathbf{p}\cdot\mathbf{r}_2/\hbar} = \int d^3r_1 d^3r_2 \langle \mathbf{p}|\mathbf{r}_1\rangle\langle \mathbf{r}_1,\sigma|O|\mathbf{r}_2,\sigma'\rangle\langle \mathbf{r}_2|\mathbf{p}\rangle = \langle \mathbf{p},\sigma|O|\mathbf{p},\sigma'\rangle .$$

Thus the integral over r space of the Wigner transform of an operator O gives the diagonal element of O in the momentum p-space representation, i.e.,

$$O_{\sigma}^{\sigma'}(\mathbf{p})=\langle \mathbf{p},\sigma|O|\mathbf{p},\sigma'\rangle = \frac{1}{(2\pi\hbar)^3}\int d^3r O_{\sigma}^{\sigma'}(\mathbf{r},\mathbf{p}) \tag{20}$$

We can generalize this relation to the similar form as in Eq. (16). Using Eq. (4), we can show the following relation:

$$O_{\sigma}^{\sigma'}(\mathbf{p}_1,\mathbf{p}_2)=\langle \mathbf{p}_1,\sigma|O|\mathbf{p}_2,\sigma'\rangle = \frac{1}{(2\pi\hbar)^3}\int d^3r d^3p\, e^{-i(\mathbf{p}_1-\mathbf{p}_2)\cdot\mathbf{r}/\hbar} \times O_{\sigma}^{\sigma'}(\mathbf{r},\mathbf{p})\delta\left[\mathbf{p}-\frac{\mathbf{p}_1+\mathbf{p}_2}{2}\right] . \tag{21}$$

Equation (20) is a special case of Eq. (21) with $\mathbf{p}_1=\mathbf{p}_2=\mathbf{p}$. The transformation, Eq. (21), of the Wigner function $f(\mathbf{r},\mathbf{p},t)$, considering the $(2\pi\hbar)^3$ factor, becomes the p-space representation of the density matrix $g(\mathbf{p}_1,\mathbf{p}_2)$ at t. Integrating the Wigner function $f(\mathbf{r},\mathbf{p},t)$ over r space, we get

$$g(\mathbf{p},t)=\int d^3r f(\mathbf{r},\mathbf{p},t) . \tag{22}$$

Equation (21) is also an inverse transformation which transforms phase space representation of an operator into momentum space representation. Defining the second kind Wigner transformation as

$$O_{\sigma}^{\sigma'}(\mathbf{r},\mathbf{p})=\int d^3q e^{i\mathbf{q}\cdot\mathbf{r}/\hbar}\langle \mathbf{p}+\mathbf{q}/2,\sigma|O|\mathbf{p}-\mathbf{q}/2,\sigma'\rangle = \int d^3p_1 d^3p_2 e^{i(\mathbf{p}_1-\mathbf{p}_2)\cdot\mathbf{r}/\hbar}\langle \mathbf{p}_1,\sigma|O|\mathbf{p}_2,\sigma'\rangle \times \delta\left[\mathbf{p}-\frac{\mathbf{p}_1+\mathbf{p}_2}{2}\right] , \tag{23}$$

Eq. (21) is the inverse transformation of this second kind Wigner transformation. The $O_{\sigma}^{\sigma'}(\mathbf{r},\mathbf{p})$ in Eqs. (4) and (23) are the same. Thus we can call Eq. (21) the second kind inverse Wigner transformation. To discriminate from this second kind transformation, if necessary, we will call the ordinary Wigner transformation (4) and the inverse Wigner transformation (16) by first kind transformations. Otherwise, we will keep the original name for the first kind transformations. The first kind Wigner transformation (4) transforms an operator from the coordinate space representation to the phase space representation. The second kind Wigner transformation (23) transforms an operator from the momentum space representation to the phase space representation. Applying the second kind inverse Wigner transformation Eq. (21) to Eq. (14), we get the density matrix condition (2) in p representation as

$$\int d^3p_1 g(\mathbf{p},\mathbf{p}_1)g(\mathbf{p}_1,\mathbf{p}')=g(\mathbf{p},\mathbf{p}') . \tag{24}$$

Similarly, the second kind inverse Wigner transform of Eq. (12) becomes the p representation of the TDHF equation (3) and the integral over r space of Eq. (12),

specifically, gives time evolution of the density $g(\mathbf{p})$ in the momentum space.

Inverse Wigner transformations [Eqs. (16) and (21)] of Eq. (12) give the TDHF equation (3). Specifically, integrating Eq. (12) over momentum space, we get back to the r representation of the TDHF equation for the local density $\rho(\mathbf{r})$. Integrating over r space, we get the p representation of the TDHF equation for $g(\mathbf{p})$. In quantum theory, only one of $\mathbf{r}$ and $\mathbf{p}$ is an independent quantum variable due to the commutation relation

$$[x_i,p_j]=i\hbar\delta_{i,j} \ . \tag{25}$$

Equation (12) is the phase space representation of the TDHF equation (3) treating $\mathbf{r}$ and $\mathbf{p}$ as independent classical variables, i.e., $\mathbf{r}$ and $\mathbf{p}$ commute each other. Thus, ∇ and ∇_p in Eqs. (11)–(15) also commute each other in this six-dimensional phase space representation. Of course, each component of $\mathbf{r}$ ($\mathbf{p}$) does not commute with the corresponding component of ∇ (∇_p). However, this phase space representation has all the quantum aspects of the system. By integrating over $\mathbf{r}$ or $\mathbf{p}$, or through inverse Wigner transformations more generally, we get back to the usual quantum theory for the TDHF approximation. Since ∇ and ∇_p in the phase space commute with each other, integrating by parts and dropping the integral of total divergence, we get

$$\begin{aligned}\int d^3pG_1(\mathbf{r},\mathbf{p})(\nabla\cdot\nabla_p-\nabla_p\cdot\nabla)^{m+1}G_2(\mathbf{r},\mathbf{p})&=\int d^3p\{[\nabla G_1(\mathbf{r},\mathbf{p})]\cdot\nabla_p-[\nabla_pG_1(\mathbf{r},\mathbf{p})]\cdot\nabla\}[(\overleftarrow{\nabla}\cdot\overrightarrow{\nabla}_p-\overleftarrow{\nabla}_p\cdot\overrightarrow{\nabla})^mG_2(\mathbf{r},\mathbf{p})]\\&=\int d^3p\{-[\nabla\cdot\nabla_pG_1(\mathbf{r},\mathbf{p})]-[\nabla_pG_1(\mathbf{r},\mathbf{p})]\cdot\nabla\}[(\overleftarrow{\nabla}\cdot\overrightarrow{\nabla}_p-\overleftarrow{\nabla}_p\cdot\overrightarrow{\nabla})^mG_2(\mathbf{r},\mathbf{p})]\\&=-\nabla\cdot\int d^3p[\nabla_pG_1(\mathbf{r},\mathbf{p})](\overleftarrow{\nabla}\cdot\overrightarrow{\nabla}_p-\overleftarrow{\nabla}_p\cdot\overrightarrow{\nabla})^mG_2(\mathbf{r},\mathbf{p}) \ ,\end{aligned} \tag{26}$$

for arbitrary functions G_1 and G_2 in phase space and for $m\geq 0$. Similarly,

$$\begin{aligned}&\int d^3rG_1(\mathbf{r},\mathbf{p})(\overleftarrow{\nabla}\cdot\overrightarrow{\nabla}_p-\overleftarrow{\nabla}_p\cdot\overrightarrow{\nabla})^{m+1}G_2(\mathbf{r},\mathbf{p})\\&\quad=\nabla_p\cdot\int d^3r[\nabla G_1(\mathbf{r},\mathbf{p})](\overleftarrow{\nabla}\cdot\overrightarrow{\nabla}_p-\overleftarrow{\nabla}_p\cdot\overrightarrow{\nabla})^mG_2(\mathbf{r},\mathbf{p}) \ .\end{aligned} \tag{27}$$

Equations (26) and (27) are total divergences in r and p space, respectively. Thus, we also have

$$\int d^3rd^3pG_1(\mathbf{r},\mathbf{p})(\overleftarrow{\nabla}\cdot\overrightarrow{\nabla}_p-\overleftarrow{\nabla}_p\cdot\overrightarrow{\nabla})^{m+1}G_2(\mathbf{r},\mathbf{p})=0 \ . \tag{28}$$

Equation (12) together with the condition of Eq. (14) for the Wigner function is a representation of TDHF in a six-dimensional phase space. Solving Eq. (12) for $f(\mathbf{r},\mathbf{p},t)$ and satisfying Eq. (14) is equivalent to solving Eq. (3) satisfying Eq. (2). Once we know the Wigner function $f(\mathbf{r},\mathbf{p},t)$ of a system, the inverse Wigner transformation of $f(\mathbf{r},\mathbf{p},t)$ gives the density matrix. The local density can be expressed by the Wigner function through Eq. (18). The expectation value of an operator O and its time evolution in the system can be found by

$$\begin{aligned}\langle O\rangle=\mathrm{Tr}(O\rho)&=\int d^3r(O\rho)(\mathbf{r})\\&=\int d^3r\int d^3p(O\rho)(\mathbf{r},\mathbf{p})\\&=\int d^3r\int d^3pO(\mathbf{r},\mathbf{p})f(\mathbf{r},\mathbf{p}) \ ,\end{aligned} \tag{29}$$

$$i\hbar\frac{d}{dt}\langle O\rangle=\mathrm{Tr}\left[Oi\hbar\frac{\partial\rho}{\partial t}\right]=\mathrm{Tr}(O[H,\rho])=-\mathrm{Tr}([H,O]\rho) \ . \tag{30}$$

Here Tr means a trace of a matrix representing an operator in a representation. For the last equality of Eq. (29), Eqs. (11) and (28) are used.

III. THE TEST PARTICLE METHOD

Solving Eq. (12) in a six-dimensional phase space is no easier than solving Eq. (1) which is in three-dimensional coordinate space. Introducing packets $F_i(\mathbf{r}-\mathbf{r}_i(t),\mathbf{p}-\mathbf{p}_i(t))$ which are centered at $\mathbf{r}_i(t)$ and $\mathbf{p}_i(t)$ in phase space and normalized by

$$\int d^3rd^3pF_i(\mathbf{r}-\mathbf{r}_i(t),\mathbf{p}-\mathbf{p}_i(t))=1 \ , \tag{31}$$

we can represent the Wigner function $f(\mathbf{r},\mathbf{p},t)$ as

$$f(\mathbf{r},\mathbf{p},t)=\frac{A}{N}\sum_{i=1}^{N}F_i(\mathbf{r}-\mathbf{r}_i(t),\mathbf{p}-\mathbf{p}_i(t)) \ . \tag{32}$$

Here A is the number of nucleons in a system and N is the total number of packets. The packets $F_i(\mathbf{r}-\mathbf{r}_i(t),\mathbf{p}-\mathbf{p}_i(t))$ can be negative at some region in the phase space and can have different forms for different packets. One such example is the choice of F_i to be the Wigner transform of $\psi_\alpha^*(\mathbf{r})\psi_\alpha(\mathbf{r}')$, where the ψ_α's are wave functions.[10] In general, we can use different normalization constants $\mathcal{N}_i$ of F_i in Eq. (31) instead of $\mathcal{N}_i=1$, and we can allow change in the form of F_i and the normalization constant $\mathcal{N}_i$ in time with the condition of $\sum_{i=1}^{N}\mathcal{N}_i(t)=N$. With these general packets we can represent the time-dependent Wigner function f exactly, however, its time evolution is too complicated. Thus, we fix $F_i(\mathbf{r},\mathbf{p})$ unchanged in time with $\mathcal{N}_i=1$. If we consider only the collective behavior of a nuclear system, we may not lose generality through these restrictions since we are not interested in the details of each single nucleon wave function. These fixed packets are called "test particles" or "pseudoparticles" with form factor $F_i(\mathbf{r},\mathbf{p})$ in the phase space. With infinitely large N, we can still represent the Wigner function f exactly at given time using proper form factors F_i. Usually, BUU calculations

use a finite number (N) of test particles with the same form factor $F_i=F$, i.e., "identical test particles." The time evolution of f is determined through the time evolution of the center $\mathbf{r}_i(t)$ and $\mathbf{p}_i(t)$ of each test particle. The time dependence of $\mathbf{r}_i$ and $\mathbf{p}_i$ should follow Eq. (12). Of course, the distribution of $\mathbf{r}_i$ and $\mathbf{p}_i$ should satisfy the TDHF density condition (14).

Let us consider Eq. (12) first. Since all the time dependencies of the Wigner function in the test particle method are represented only through the time dependencies of $\mathbf{r}_i$ and $\mathbf{p}_i$ in Eq. (32), Eq. (13) can be rewritten as, dropping the common normalization factor A/N,

$$-\sum_i \left[\frac{\partial \mathbf{r}_i(t)}{\partial t}\cdot\nabla+\frac{\partial \mathbf{p}_i(t)}{\partial t}\cdot\nabla_p\right]F_i(\mathbf{r}-\mathbf{r}_i(t),\mathbf{p}-\mathbf{p}_i(t))-\sum_i\{[\nabla H(\mathbf{r},\mathbf{p})]\cdot\nabla_p-[\nabla_p H(\mathbf{r},\mathbf{p})]\cdot\nabla\}F_i(\mathbf{r}-\mathbf{r}_i(t),\mathbf{p}-\mathbf{p}_i(t))$$
$$=\sum_i\sum_{n=1}^{\infty}\frac{(-1)^n}{(2n+1)!}\left[\frac{\hbar}{2}\right]^{2n}H(\mathbf{r},\mathbf{p})(\overleftarrow{\nabla}\cdot\vec{\nabla}_p-\overleftarrow{\nabla}_p\cdot\vec{\nabla})^{2n+1}F_i(\mathbf{r}-\mathbf{r}_i(t),\mathbf{p}-\mathbf{p}_i(t))\ . \quad (33)$$

This is the equation of motion for $\mathbf{r}_i(t)$ and $\mathbf{p}_i(t)$ in the six-dimensional phase space which retains all the information about quantum effects as in TDHF. In this equation, $\mathbf{r}_i(t)$ and $\mathbf{p}_i(t)$ are coupled and expressed in the six-dimensional phase space. From Eq. (33), we can extract the time evolution of $\mathbf{r}_i(t)$ and $\mathbf{p}_i(t)$ in a quantum description of the system.

As we discussed in Sec. II, we can get the usual quantum description corresponding to Eq. (33) through the integral over p or r space, or more generally, through inverse Wigner transformations. Let us consider the integral over p space of Eq. (33) first. Since $\mathbf{r}_i$ and $\mathbf{p}_i$ are independent of $\mathbf{r}$ and $\mathbf{p}$, using Eq. (26), the integral over p space of Eq. (33) becomes

$$\nabla\cdot\sum_i\int d^3p\left[-\frac{\partial \mathbf{r}_i(t)}{\partial t}+[\nabla_p H(\mathbf{r},\mathbf{p})]\right]F_i(\mathbf{r}-\mathbf{r}_i(t),\mathbf{p}-\mathbf{p}_i(t))$$
$$=-\nabla\cdot\sum_i\sum_{n=1}^{\infty}C_n\int d^3p[\nabla_p H(\mathbf{r},\mathbf{p})](\overleftarrow{\nabla}\cdot\vec{\nabla}_p-\overleftarrow{\nabla}_p\cdot\vec{\nabla})^{2n}F_i(\mathbf{r}-\mathbf{r}_i(t),\mathbf{p}-\mathbf{p}_i(t))\ . \quad (34)$$

This is a quantum description of the equation of motion for the $\mathbf{r}_i(t)$ in r-space representation. Similarly, the integral over r space of Eq. (33) becomes

$$\nabla_p\cdot\sum_i\int d^3r\left[-\frac{\partial \mathbf{p}_i(t)}{\partial t}-[\nabla H(\mathbf{r},\mathbf{p})]\right]F_i(\mathbf{r}-\mathbf{r}_i(t),\mathbf{p}-\mathbf{p}_i(t))$$
$$=\nabla_p\cdot\sum_i\sum_{n=1}^{\infty}C_n\int d^3r[\nabla H(\mathbf{r},\mathbf{p})](\overleftarrow{\nabla}\cdot\vec{\nabla}_p-\overleftarrow{\nabla}_p\cdot\vec{\nabla})^{2n}F_i(\mathbf{r}-\mathbf{r}_i(t),\mathbf{p}-\mathbf{p}_i(t))\ . \quad (35)$$

This is a quantum description of the equation of motion for the $\mathbf{p}_i(t)$ in p-space representation. The integral over r space of Eq. (34) and the integral over p space of Eq. (35) are both zero. These represent the particle number conservation in TDHF, i.e., trace of Eq. (3) is zero. Equations (34) and (35) are TDHF equations for the density in r and p space, respectively, in terms of the time-dependent basis functions $F_i(\mathbf{r}-\mathbf{r}_i(t),\mathbf{p}-\mathbf{p}_i(t))$.

Since ∇ is the common factor in Eq. (34) and ∇_p is the common factor in Eq. (35), these equations can be rewritten as

$$\sum_i\int d^3p\left[-\frac{\partial \mathbf{r}_i(t)}{\partial t}+[\nabla_p H(\mathbf{r},\mathbf{p})]\right]F_i(\mathbf{r}-\mathbf{r}_i(t),\mathbf{p}-\mathbf{p}_i(t))+\mathbf{C}_r$$
$$=-\sum_i\sum_{n=1}^{\infty}C_n\int d^3p[\nabla_p H(\mathbf{r},\mathbf{p})](\overleftarrow{\nabla}\cdot\vec{\nabla}_p-\overleftarrow{\nabla}_p\cdot\vec{\nabla})^{2n}F_i(\mathbf{r}-\mathbf{r}_i(t),\mathbf{p}-\mathbf{p}_i(t))\ , \quad (36)$$

$$\sum_i\int d^3r\left[\frac{\partial \mathbf{p}_i(t)}{\partial t}+[\nabla H(\mathbf{r},\mathbf{p})]\right]F_i(\mathbf{r}-\mathbf{r}_i(t),\mathbf{p}-\mathbf{p}_i(t))+\mathbf{C}_p$$
$$=-\sum_i\sum_{n=1}^{\infty}C_n\int d^3r[\nabla H(\mathbf{r},\mathbf{p})](\overleftarrow{\nabla}\cdot\vec{\nabla}_p-\overleftarrow{\nabla}_p\cdot\vec{\nabla})^{2n}F_i(\mathbf{r}-\mathbf{r}_i(t),\mathbf{p}-\mathbf{p}_i(t))\ . \quad (37)$$

Here, $\mathbf{C}_r$ and $\mathbf{C}_p$ are constants in r and p variables. These equations are the quantum equations of motion of $\mathbf{r}_i(t)$ and $\mathbf{p}_i(t)$ with unknown constants $\mathbf{C}_r$ and $\mathbf{C}_p$. We will come back to these constants later. In Eqs. (36) and (37), $\mathbf{r}$ and $\mathbf{p}$ are the independent quantum variables, respectively, and $\mathbf{r}_i(t)$ and $\mathbf{p}_i(t)$ are parameters characterizing the centers of test particles.

Now consider the integral over r space of Eq. (36) and the integral over p space of Eq. (37) which are nothing but the expectation values for the corresponding operators in a quantum description. Due to Eq. (28), the right-hand sides of Eqs. (36) and (37) have zero integrals over r and p space, respectively. Except the constant terms ($\mathbf{C}_r$ and $\mathbf{C}_p$), all other

terms in Eqs. (36) and (37) have finite integrals over r and p space since they are physical quantities. Thus $\mathbf{C}_r$ and $\mathbf{C}_p$ are necessarily zero. Finally, since $\mathbf{r}_i$ and $\mathbf{p}_i$ are independent of $\mathbf{r}$ and $\mathbf{p}$, using Eq. (31), we get

$$\sum_i \left[-\frac{\partial \mathbf{r}_i(t)}{\partial t} + \int d^3r d^3p [\nabla_p H(\mathbf{r},\mathbf{p})] F_i(\mathbf{r}-\mathbf{r}_i(t),\mathbf{p}-\mathbf{p}_i(t)) \right] = 0 , \tag{38}$$

$$\sum_i \left[\frac{\partial \mathbf{p}_i(t)}{\partial t} + \int d^3r d^3p [\nabla H(\mathbf{r},\mathbf{p})] F_i(\mathbf{r}-\mathbf{r}_i(t),\mathbf{p}-\mathbf{p}_i(t)) \right] = 0 . \tag{39}$$

Equations (38) and (39) are the equations of motion for $\mathbf{r}_i(t)$ and $\mathbf{p}_i(t)$, i.e., for the motion of test particles. Notice here that these equations are necessary but not sufficient conditions of Eqs. (34) and (35).

Now let us consider the physical meaning of Eqs. (38) and (39). First consider the inverse Wigner transform of $[\nabla_p H(\mathbf{r},\mathbf{p})]$. From Eq. (16), integrating by part and dropping the integral of total divergence,

$$\frac{1}{(2\pi\hbar)^3} \int d^3p d^3r e^{i\mathbf{p}\cdot(\mathbf{r}_1-\mathbf{r}_2)/\hbar} [\nabla_p H(\mathbf{r},\mathbf{p})] \delta\left(\mathbf{r}-\frac{\mathbf{r}_1+\mathbf{r}_2}{2}\right) = \frac{1}{(2\pi\hbar)^3} \int d^3p d^3r e^{i\mathbf{p}\cdot(\mathbf{r}_1-\mathbf{r}_2)/\hbar} \frac{i(\mathbf{r}_2-\mathbf{r}_1)}{\hbar} H(\mathbf{r},\mathbf{p}) \delta\left(\mathbf{r}-\frac{\mathbf{r}_1+\mathbf{r}_2}{2}\right)$$

$$= \frac{i}{\hbar} \langle \mathbf{r}_1,\sigma | (H\mathbf{r}_2 - \mathbf{r}_1 H) | \mathbf{r}_2,\sigma' \rangle = \frac{i}{\hbar} \langle \mathbf{r}_1,\sigma | [H,\hat{\mathbf{r}}] | \mathbf{r}_2,\sigma' \rangle ,$$

where $\hat{\mathbf{r}}$ is an operator representing the position vector. Thus $[-i\hbar\nabla_p H(\mathbf{r},\mathbf{p})]$ is a Wigner transform of the commutator $[H,\hat{\mathbf{r}}]$, i.e.,

$$[\nabla_p H(\mathbf{r},\mathbf{p})] = \int d^3s e^{-i\mathbf{p}\cdot\mathbf{s}/\hbar} \langle \mathbf{r}+\mathbf{s}/2,\sigma | \frac{i}{\hbar} [H,\hat{\mathbf{r}}] | \mathbf{r}-\mathbf{s}/2,\sigma' \rangle . \tag{40}$$

Similarly, the inverse Wigner transform of $[\nabla H(\mathbf{r},\mathbf{p})]$ becomes, from Eq. (16) and using the integral property of the gradient of the delta function,

$$\frac{1}{(2\pi\hbar)^3} \int d^3p d^3r e^{i\mathbf{p}\cdot(\mathbf{r}_1-\mathbf{r}_2)/\hbar} [\nabla H(\mathbf{r},\mathbf{p})] \delta\left(\mathbf{r}-\frac{\mathbf{r}_1+\mathbf{r}_2}{2}\right) = \frac{-1}{(2\pi\hbar)^3} (\nabla_1+\nabla_2) \int d^3p d^3r e^{i\mathbf{p}\cdot(\mathbf{r}_1-\mathbf{r}_2)/\hbar} H(\mathbf{r},\mathbf{p}) \delta\left(\mathbf{r}-\frac{\mathbf{r}_1+\mathbf{r}_2}{2}\right)$$

$$= -\langle \mathbf{r}_1,\sigma | (\overleftarrow{\nabla} H + H\overrightarrow{\nabla}) | \mathbf{r}_2,\sigma' \rangle = -\langle \mathbf{r}_1,\sigma | (-\overleftarrow{\nabla} H + H\overrightarrow{\nabla}) | \mathbf{r}_2,\sigma' \rangle$$

$$= -\langle \mathbf{r}_1,\sigma | [H,\nabla] | \mathbf{r}_2,\sigma' \rangle .$$

Here $-i\hbar\nabla$ is the r-space representation of the momentum vector operator $\hat{\mathbf{p}}$. Thus $[i\hbar\nabla H(\mathbf{r},\mathbf{p})]$ is a Wigner transform of the commutator $[H,\hat{\mathbf{p}}] = -i\hbar[H,\nabla]$, i.e.,

$$[\nabla H(\mathbf{r},\mathbf{p})] = -\int d^3s e^{-i\mathbf{p}\cdot\mathbf{s}/\hbar} \langle \mathbf{r}+\mathbf{s}/2,\sigma | [H,\nabla] | \mathbf{r}-\mathbf{s}/2,\sigma' \rangle . \tag{41}$$

We can get the same relation using the second kind transformations Eqs. (21) and (23).

Since $[\nabla_p H(\mathbf{r},\mathbf{p})]$ is the Wigner transform of operator $i/\hbar[H,\hat{\mathbf{r}}]$ [Eq. (40)], using Eqs. (32), (29), and (30), the last term of Eq. (38) becomes

$$\sum_i \int d^3r d^3p [\nabla_p H(\mathbf{r},\mathbf{p})] F_i(\mathbf{r}-\mathbf{r}_i(t),\mathbf{p}-\mathbf{p}_i(t))$$

$$= \frac{N}{A} \int d^3r \frac{i}{\hbar} [H,\hat{\mathbf{r}}] \rho(\mathbf{r}) = \frac{N}{A} \frac{i}{\hbar} \mathrm{Tr}([H,\hat{\mathbf{r}}]\rho)$$

$$= \frac{N}{A} \frac{d}{dt} \langle \hat{\mathbf{r}} \rangle . \tag{42}$$

This is the relation connecting the time evolution of the expectation value of an operator $\hat{\mathbf{r}}$, which is the c.m. coordinate $\langle \hat{\mathbf{r}} \rangle$ of the system, to the c.m. velocity of the system, i.e., the expectation value of nucleon field velocity operator $\mathcal{V}$ in a mean-field Hamiltonian H, which is represented by $\mathcal{V}(\mathbf{r},\mathbf{p}) = [\nabla_p H(\mathbf{r},\mathbf{p})]$ in the phase space. Similarly, the last term of Eq. (39) becomes

$$\sum_i \int d^3r d^3p [\nabla H(\mathbf{r},\mathbf{p})] F_i(\mathbf{r}-\mathbf{r}_i(t),\mathbf{p}-\mathbf{p}_i(t))$$

$$= -\frac{N}{A} \int d^3r [H,\nabla] \rho(\mathbf{r})$$

$$= -\frac{N}{A} \mathrm{Tr}([H,\nabla]\rho)$$

$$= -\frac{i}{\hbar} \frac{N}{A} \mathrm{Tr}([H,\hat{\mathbf{p}}]\rho) = -\frac{N}{A} \frac{d}{dt} \langle \hat{\mathbf{p}} \rangle . \tag{43}$$

This is the relation connecting the time evolution of the expectation value of an operator $\hat{\mathbf{p}}$, which is the c.m. momentum $\langle \hat{\mathbf{p}} \rangle$ of the system, to the total force acting on the system, i.e., the expectation value of force operator $\mathcal{F}$ of nucleon field in a mean-field Hamiltonian H, which is represented by $\mathcal{F}(\mathbf{r},\mathbf{p}) = -[\nabla H(\mathbf{r},\mathbf{p})]$ in the phase space. Using Eqs. (42), (43), and (32), Eqs. (38) and (39) can be rewritten as

$$\frac{d}{dt}\langle\hat{\mathbf{r}}\rangle=\frac{A}{N}\sum_i\frac{\partial\mathbf{r}_i(t)}{\partial t}$$
$$=\langle\mathcal{V}\rangle=\int d^3rd^3p[\nabla_pH(\mathbf{r},\mathbf{p})]f(\mathbf{r},\mathbf{p},t)\ , \quad (44)$$
$$\frac{d}{dt}\langle\hat{\mathbf{p}}\rangle=\frac{A}{N}\sum_i\frac{\partial\mathbf{p}_i(t)}{\partial t}$$
$$=\langle\mathcal{F}\rangle=-\int d^3rd^3p[\nabla H(\mathbf{r},\mathbf{p})]f(\mathbf{r},\mathbf{p},t)\ . \quad (45)$$

These equations represent that the time evolution of the c.m. coordinate and momentum of the system can be represented by the time evolution of the centers $\mathbf{r}_i(t)$ and $\mathbf{p}_i(t)$ of the test particles, respectively. The c.m. motion of the system follows classical dynamics with the average mean-field velocity $\langle\mathcal{V}\rangle$ and force $\langle\mathcal{F}\rangle$ of the system in a quantum description. This quantum description of c.m. motion is well known. The test particle method for the quantum extended Vlasov equation (12) correctly describes the motion of c.m. coordinates through Eqs. (44) and (45) and the motion of test particles through Eqs. (38) and (39) in a quantum description.

In Eqs. (38) and (39), all the test particles are coupled through the summation. However, if these equations are satisfied for each test particle separately, i.e.,

$$\frac{\partial\mathbf{r}_i(t)}{\partial t}=\int d^3rd^3p[\nabla_pH(\mathbf{r},\mathbf{p})]F_i(\mathbf{r}-\mathbf{r}_i(t),\mathbf{p}-\mathbf{p}_i(t))$$
$$=\int d^3rd^3pH(\mathbf{r},\mathbf{p})\nabla_{p_i}F_i(\mathbf{r}-\mathbf{r}_i(t),\mathbf{p}-\mathbf{p}_i(t))\ , \quad (46)$$
$$\frac{\partial\mathbf{p}_i(t)}{\partial t}=\int d^3rd^3p[\nabla H(\mathbf{r},\mathbf{p})]F_i(\mathbf{r}-\mathbf{r}_i(t),\mathbf{p}-\mathbf{p}_i(t))$$
$$=\int d^3rd^3pH(\mathbf{r},\mathbf{p})\nabla_iF_i(\mathbf{r}-\mathbf{r}_i(t),\mathbf{p}-\mathbf{p}_i(t))\ , \quad (47)$$

then Eqs. (38) and (39) are automatically satisfied. Here, ∇_i and ∇_{p_i} mean the gradients respect to $\mathbf{r}_i$ and $\mathbf{p}_i$. Equations (46) and (47) are sufficient but not necessary conditions for Eqs. (38) and (39). These equations represent that the time evolution of the centers $\mathbf{r}_i(t)$ and $\mathbf{p}_i(t)$ of the ith test particle follow classical dynamics[11,12] with averaged mean-field velocity $\langle\mathcal{V}\rangle_i$ and force $\langle\mathcal{F}\rangle_i$ over the packet $F_i(\mathbf{r}-\mathbf{r}_i(t),\mathbf{p}-\mathbf{p}_i(t))$ of the test particle. These are equations of motion of test particles in a full quantum description obtained by using Eq. (12) without truncation in $\hbar$ order and are the same as in Ref. 7 which is a classical limit considering Eq. (9) without higher-order terms in $\hbar$. Once we start with the proper initial distribution of test particles described by the proper form factor $F_i(\mathbf{r},\mathbf{p})$ for a system with mean-field Hamiltonian H, the time evolution of test particles is determined through Eqs. (46) and (47). Then, we know the Wigner function $f(\mathbf{r},\mathbf{p},t)$ of the system through Eq. (32). The inverse Wigner transform of the Wigner function becomes a density matrix. Specifically, the local density can be expressed by the Wigner function thrugh Eq. (18). The expectation value of an operator O and its time evolution in the system can be found by Eqs. (29) and (30), respectively. This is an exact quantum description of the system except we have used sufficient but not necessary conditions, Eqs. (46) and (47), for Eqs. (38) and (39).

Up to now we have considered only Eq. (12) which is the Wigner transform of the TDHF equation (3). In TDHF we have density matrix condition, Eq. (2), which is represented by Eq. (14) in a phase space. Thus, for this to be a correct quantum description, the distribution of test particles with form factor $F_i(\mathbf{r},\mathbf{p})$ should be restricted to properly represent the Wigner function $f(\mathbf{r},\mathbf{p},t)$ which should satisfy the Pauli principle. The details of the system using the test particle method entirely depend on the restriction on the distribution of test particles incorporated with the form factor $F_i(\mathbf{r},\mathbf{p})$ of the test particle. The density matrix condition (14) gives special restriction on the distribution of test particles and on the form factor $F_i(\mathbf{r},\mathbf{p})$. Using Eqs. (7) and (32), Eq. (15) becomes,

$$\sum_i F_i(\mathbf{r}-\mathbf{r}_i(t),\mathbf{p}-\mathbf{p}_i(t))\left[\frac{A}{N}\frac{(2\pi\hbar)^3}{4}\sum_j F_j(\mathbf{r}-\mathbf{r}_j(t),\mathbf{p}-\mathbf{p}_j(t))-1\right]$$
$$=\sum_i\sum_j\sum_{n=1}^{\infty}C_n'F_i(\mathbf{r}-\mathbf{r}_i(t),\mathbf{p}-\mathbf{p}_i(t))(\overleftarrow{\nabla}\cdot\vec{\nabla}_p-\overleftarrow{\nabla}_p\cdot\vec{\nabla})^{2n}F_j(\mathbf{r}-\mathbf{r}_j(t),\mathbf{p}-\mathbf{p}_j(t))\ , \quad (48)$$
$$C_n'=\frac{A}{N}\frac{(2\pi\hbar)^3}{4}\frac{(-1)^n}{(2n)!}\left[\frac{\hbar}{2}\right]^{2n}\ .$$

The right-hand side of Eq. (48) has zero integral over phase space due to Eq. (28). Thus, using the normalization condition (31), from Eq. (48) we get

$$\frac{A}{N^2}\frac{(2\pi\hbar)^3}{4}\sum_i\sum_j\int d^3rd^3pF_i(\mathbf{r}-\mathbf{r}_i(t),\mathbf{p}-\mathbf{p}_i(t))F_j(\mathbf{r}-\mathbf{r}_j(t),\mathbf{p}-\mathbf{p}_j(t))=\frac{1}{N}\sum_{i=1}^{N}1=1\ . \quad (49)$$

The density matrix condition (14) gives the constraint on the distribution of test particles of form factor $F_i(\mathbf{r},\mathbf{p})$ through this overlap integral. This condition [Eq. (49)] is the same for the classical limit case [Eq. (8)] and can be implemented through the proper distribution of test particles ($\mathbf{r}_i$ and $\mathbf{p}_i$) incorporated with the form factor normalized by Eq. (31). However, since Eq. (49) is not a local constraint in the phase space, this is a necessary but not sufficient condition for the density matrix condition Eqs. (14) or (8), which are local conditions in phase space.

The conditions, Eqs. (8) and (14), discriminate between classical limit and quantum case. With a proper distribution of $\mathbf{r}_i$ and $\mathbf{p}_i$ satisfying the condition of Eq. (49), the form factor $F_i(\mathbf{r},\mathbf{p})=\delta(\mathbf{r})\delta(\mathbf{p})$ or $F_i(\mathbf{r},\mathbf{p})\propto\theta(a(\mathbf{r})-p)$ satisfies Eq. (8), which is a classical limit, but does not satisfy Eq. (14). This means that the discrimination between the quantum description and the classical limit can depend on the choice of the form factor $F_i(\mathbf{r},\mathbf{p})$ as well as the distribution of test particles.

The local conditions in six-dimensional phase space for Eq. (14) of the quantum case or for Eq. (8) of the classical limit case are very difficult to implement in the test particle method. Even for the global condition (49), it is hard to find the correct constraints on the distribution of test particles with the form factor through which this global condition is maintained in the time evolution. Thus, we relax the Slater determinant condition (2) by requesting only the Pauli condition, which is represented in a phase space by

$$\tilde{f}^2\le|\tilde{f}| \ . \tag{50}$$

For this case, the overlap condition (49) for the distribution of test particles with the form factor $F_i(\mathbf{r},\mathbf{p})$ will also be relaxed to

$$\frac{A}{N^2}\frac{(2\pi\hbar)^3}{4}\sum_i\sum_j\int d^3rd^3pF_i(\mathbf{r}-\mathbf{r}_i(t),\mathbf{p}-\mathbf{p}_i(t))\times F_j(\mathbf{r}-\mathbf{r}_j(t),\mathbf{p}-\mathbf{p}_j(t))\le 1 \ . \tag{51}$$

This kind of relaxation of Slater determinant condition has also been used in the usual quantum description of the nuclear system. In the random-phase approximation (RPA), BCS pairing, or extended TDHF, the wave function of the system is no longer a single Slater determinant and thus the density matrix condition (2) is not valid. Instead, we have $\rho^2\le\rho$ in a density matrix diagonalized representation. For these cases, the shell effects are smeared out through the averaging effects over the state of the system which can be represented as a linear combination of many Slater determinants. In the BCS pairing case, the shape of a nucleus depends on the gap energy. A ground-state nucleus in BCS can be a spherical shape depending on the pairing scheme even for the nucleus which has a deformed ground state in TDHF. These situations correspond to the different restrictions on the distribution of test particles and on the form factor $F_i(\mathbf{r},\mathbf{p})$ in the test particle method in a phase space. The density matrix condition (14) in TDHF is less restrictive than its classical limit, Eq. (8), and more restrictive than the Pauli condition, Eq. (50). Thus the Pauli condition, Eq. (50), is closer to the condition in Eq. (14) than to the condition in a classical limit, as in Eq. (8), and can be implemented easily through the proper distribution of test particles ($\mathbf{r}_i$ and $\mathbf{p}_i$) satisfying the condition of Eq. (51) incorporated with a specific choice of the form factor normalized by Eq. (31). Implementing this Pauli condition [Eq. (50)] is much easier than implementing the classical density matrix condition [Eq. (8)]. Therefore, this relaxation of the Slater determinant condition is what actually happened in the usual BUU calculations using the test particle method.

For the momentum-independent mean-field potential case, Eq. (10) becomes

$$H(\mathbf{r},\mathbf{p})=\frac{p^2}{2m}+U(\mathbf{r}) \ . \tag{52}$$

For this case, Eqs. (46) and (47) reduce to

$$\frac{\partial\mathbf{r}_i(t)}{\partial t}=\int d^3rd^3p\frac{\mathbf{p}}{m}F_i(\mathbf{r}-\mathbf{r}_i(t),\mathbf{p}-\mathbf{p}_i(t)) \ ,$$

$$\frac{\partial\mathbf{p}_i(t)}{\partial t}=-\int d^3rd^3p[\nabla U(\mathbf{r})]F_i(\mathbf{r}-\mathbf{r}_i(t),\mathbf{p}-\mathbf{p}_i(t)) \ .$$

The integral over p space can be done explicitly. Using the normalization condition (31), these equations become

$$\frac{\partial\mathbf{r}_i(t)}{\partial t}=\frac{\mathbf{p}_i(t)}{m} \ , \tag{53}$$

$$\frac{\partial\mathbf{p}_i(t)}{\partial t}=-\int d^3r[\nabla U(\mathbf{r})]S_i(\mathbf{r}-\mathbf{r}_i(t))=-\int d^3rU(\mathbf{r})\nabla_iS_i(\mathbf{r}-\mathbf{r}_i(t)) \ , \tag{54}$$

$$S_i(\mathbf{r}-\mathbf{r}_i(t))=\int d^3pF_i(\mathbf{r}-\mathbf{r}_i(t),\mathbf{p}-\mathbf{p}_i(t)) \ . \tag{55}$$

Here we have assumed that $F_i(\mathbf{r},\mathbf{p})$ has even parity in p space, i.e., $F_i(\mathbf{r},-\mathbf{p})=F_i(\mathbf{r},\mathbf{p})$ to get Eq. (53). Since $H(\mathbf{r},-\mathbf{p})=H(\mathbf{r},\mathbf{p})$ for the mean-field Hamiltonian of Eq. (52), the form factor F_i of the test particle may be assumed to have even parity in p space without losing generality. For the momentum-independent mean-field potential case, we need only to specify the form factor in r space $S_i(\mathbf{r})$ for the test particles instead of the form factor in the phase space $F_i(\mathbf{r},\mathbf{p})$ for the evolution of the test particles, Eqs. (53) and (54), and thus for the evolution of the system. We still need to know the form factor in p space as well, in order to evaluate the expectation value of the momentum-dependent operator such as the kinetic energy or momentum of the system. However, we can factorize the form factor into r- and p-space parts separately for this case.

In the Vlasov prescription, "identical test particles" with the following forms of $F(\mathbf{r},\mathbf{p})$ have been used.

(i) Gaussian packet with finite width in both of r and p spaces:[7]

$$F(\mathbf{r},\mathbf{p})=\frac{1}{(2\pi\hbar)^3}e^{-r^2/(2\Delta^2)}e^{-p^2\Delta^2/(2\hbar^2)} \ . \tag{56}$$

(ii) Packet with finite width in r space and zero width in p space:

$$F(\mathbf{r},\mathbf{p})=S(\mathbf{r})\delta(\mathbf{p}) \tag{57}$$

with[12]

$$S(\mathbf{r})=S(x)S(y)S(z) \ ,$$

$$S(x)=\frac{1}{b}\left[1-\frac{|x|}{b}\right]\theta\left[1-\frac{|x|}{b}\right] \ . \tag{58}$$

We can also use the spherical form for S instead of Eq. (58):

$$S(\mathbf{r})=\frac{3}{\pi b^3}\left[1-\frac{r}{b}\right]\theta\left[1-\frac{r}{b}\right] . \quad (59)$$

(iii) Point test particle, i.e., packet with zero width in both r and p spaces:[4,5] Eq. (57) with

$$S(\mathbf{r})=\delta(\mathbf{r}) . \quad (60)$$

The maximum value of the width of the packet (Δ or b) should be restricted by the surface thickness of the Wigner function $f(\mathbf{r},\mathbf{p},t)$ for a real nucleus to avoid unphysical surface. Thus, the maximum value of Δ or b is of the order of 1 fm. The minimum value of the width Δ or b should be large enough to give a smooth function $f(\mathbf{r},\mathbf{p},t)$ in r and p space. Therefore, Δ or b should be larger than the mean distance between test particles. For a smaller width of the packet, we need a larger number of test particles (larger N). For a smaller N, we need a larger width of test particles. The parameter $\gamma=\rho_0 R_S^3 N/A$ is defined in Ref. 12. Here ρ_0 is the nuclear matter saturation density and R_S is the root-mean-square radius of the packet. For $\gamma \gtrsim 25$,[12] the fluctuation in $f(\mathbf{r},\mathbf{p},t)$, due to the finite number of packets with finite width, can be neglected. This means that we require at least $N/A \approx 170$ test particles with $R_S=1$ fm for the $\rho_0=0.145$ fm^{-3} case.

IV. NUMERICAL RESULTS OF THE TEST PARTICLE METHOD

In BUU calculations, the following form of momentum-independent mean-field potential has been used:

$$U(\mathbf{r})=A\rho(\mathbf{r})+B\rho^{\sigma}(\mathbf{r})+V_0\int d^3r'\frac{e^{-|\mathbf{r}-\mathbf{r}'|/a}}{|\mathbf{r}-\mathbf{r}'|/a}\rho(\mathbf{r}') . \quad (61)$$

The test particle method of Sec. III is applied to ^{40}Ca for this mean-field potential with the following two sets of parameters:

$$A=-816.74 \text{ MeV fm}^3, \quad B=3238.1 \text{ MeV fm}^6 ,$$
$$\sigma=2, \quad V_0=0 ; \quad (62)$$

$$A=0, \quad B=3238.1 \text{ MeV fm}^6, \quad \sigma=2 ,$$
$$V_0=-668.65 \text{ MeV}, \quad a=0.45979 \text{ fm} . \quad (63)$$

The Coulomb interaction and the symmetry energy are neglected for numerical simplicity. The local force set in Eq. (62) and the Yukawa force set in Eq. (63) have the same nuclear matter properties: the binding energy of $E/A=-15.77$ MeV, the saturation density of $\rho_0=0.145$ fm^{-3}, and the compressibility of $K=368$ MeV. The self-consistent density of static Vlasov equation (9) with the mean-field potential of Eq. (61) can be found. This has been discussed in detail in Refs. 5 and 6. For the force parameter set of Eq. (62), which has local force only, the self-consistent density has a sharp surface with $\rho(\mathbf{r})=\rho_0$ inside of a sphere (see the dotted lines in the left column of Fig. 1 for ^{40}Ca). This has the binding energy of -15.77 MeV per nucleon. For the force parameter set of Eq. (63) which has a finite range Yukawa force, the self-consistent density has a diffuse surface with $\rho(\mathbf{r})=0$ outside of a sphere of finite radius R (see the dotted lines in the right column of Fig. 1 for ^{40}Ca). The binding energy of ^{40}Ca is -10.04 MeV per nucleon. On the other hand, self-consistent Hartree-Fock density for the potential Eq. (61) has a diffuse surface with an infinite tail for both of the force parameter sets [see the dashed lines in the left column of Fig. 1 for the local force, Eq. (62), and in the right column for the Yukawa force, Eq. (63)]. For Hartree-Fock density, the same code used in Ref. 13 is used for the mean-field potential of Eq. (61). The ground-state binding energy per nucleon of ^{40}Ca are -12.49 MeV for Eq. (62) and -9.12 MeV for Eq. (63).

Since we are considering the momentum-independent potential case, we need only to specify $S(\mathbf{r})$ of Eq. (55) for the evolution of the system, or equivalently, for Eqs. (53) and (54). If we choose point test particles for the form factor, i.e.,

$$F(\mathbf{r}-\mathbf{r}_i,\mathbf{p}-\mathbf{p}_i)=S(\mathbf{r}-\mathbf{r}_i)\delta(\mathbf{p}-\mathbf{p}_i) ,$$
$$S(\mathbf{r}-\mathbf{r}_i)=\delta(\mathbf{r}-\mathbf{r}_i) , \quad (64)$$

Eq. (54) can be simplified as

$$\frac{\partial \mathbf{p}_i(t)}{\partial t}=-[\nabla U(\mathbf{r})]_{\mathbf{r}=\mathbf{r}_i} . \quad (65)$$

For the potential $U(\mathbf{r})$ in Eq. (65), we require to calculate the local density $\rho(\mathbf{r})$ which is, from Eqs. (18) and (32),

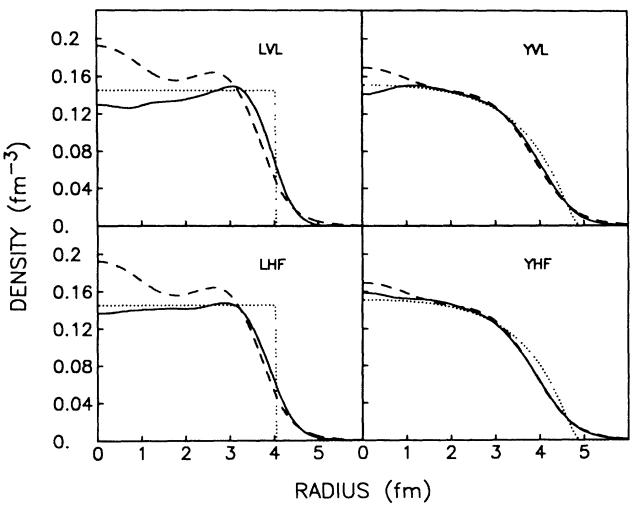

FIG. 1. Nuclear densities of ^{40}Ca. The underlying force is the local force, Eq. (62), for the cases of LVL and LHF (left column) and the Yukawa force, Eq. (63), for the cases of YVL and YHF (right column). Dotted curves are the self-consistent density of the static Vlasov equation (9) with the aforementioned force for each case. Dashed curves are the static Hartree-Fock density with corresponding force. Solid lines are the densities averaged over the time period of each evolution of a nucleus using the test particle method. The initial densities for the time evolution are the static Vlasov densities (dotted lines) for LVL and YVL, and the static Hartree-Fock densities (dashed lines) for LHF and YHF with corresponding forces. See text for details.

$$\rho(\mathbf{r})=\frac{A}{N}\sum_{i=1}^{N}S(\mathbf{r}-\mathbf{r}_i)=\frac{A}{N}\sum_{i=1}^{N}\delta(\mathbf{r}-\mathbf{r}_i)\ . \tag{66}$$

This local density is a very fluctuating function of $\mathbf{r}$ for test particles of Eq. (64) no matter how large N is. Thus, a local averaged density of Eq. (66) over a sphere centered at $\mathbf{r}$ with the radius of b is used for the density required by Eq. (65) instead of the local density. This local averaged density for point test particles is equivalent to the local density itself for test particles with the form factor of

$$S(\mathbf{r}-\mathbf{r}_i)=\frac{3}{4\pi}\frac{1}{b^3}\theta\left[1-\frac{|\mathbf{r}-\mathbf{r}_i|}{b}\right]\ . \tag{67}$$

However, these two are not equivalent for the evolution of $\mathbf{p}_i$, Eq. (54), and for the evaluation of some physical quantities such as the root-mean-square radius of the nucleus.

For the numerical evolution of Eqs. (53) and (65), $N/A=200$ test particles per nucleon has been used. The local averaged density is evaluated on the three-dimensional Cartesian grid points with the grid spacing of 1 fm averaged over the sphere with the volume of $(4\pi/3)b^3=7$ fm^3. For the local density at point $\mathbf{r}_i$ which is not on the grid point, three-point interpolation in each three Cartesian directions is used. We also need to specify the initial distribution of the test particles, i.e., $\mathbf{r}_i$ and $\mathbf{p}_i$ at $t=0$. First, the positions $\mathbf{r}_i$ for test particles are distributed stochastically according to the corresponding self-consistent density of a static nucleus. Four cases are considered here for the initial distribution.

(1) Point test particles are distributed initially such that the local density ρ of Eq. (66) depicts the self-consistent density of the static Vlasov equation with local force (dotted lines in the left column of Fig. 1). We denote this case by LVL.

(2) Point test particles are distributed initially such that the local density ρ of Eq. (66) depicts the self-consistent density of the static Hartree-Fock equation with local force (dashed lines in the left column of Fig. 1). We denote this case by LHF.

(3) Point test particles are distributed initially such that the local density ρ of Eq. (66) depicts the self-consistent density of the static Vlasov equation with Yukawa force (dotted lines in the right column of Fig. 1). We denote this case by YVL.

(4) Point test particles are distributed initially such that the local density ρ of Eq. (66) depicts the self-consistent density of the static Hartree-Fock equation with Yukawa force (dashed lines in the right column of Fig. 1). We denote this case by YHF.

Then, for each case, the momentum $\mathbf{p}_i$ of the ith particle has been assigned randomly in a Fermi sphere with a radius of local Fermi momentum. In each case, the nucleus has been evolved through Eqs. (53) and (65) with the corresponding potential up to $t=180$ fm/c with the time step of $\Delta t=0.3$ fm/c. In these calculations, the energy of a nucleus increased by about 2 MeV per nucleon for local forces (LVL and LHF) and about 1.5 MeV per nucleon for Yukawa forces (YVL and YHF) at $t=180$ fm/c due to the numerical inaccuracy. The binding energies per nucleon were -13.1 MeV for LVL, -12.1 MeV for LHF, -9.4 MeV for YVL, and -8.9 MeV for YHF initially (at $t=0$) in these calculations which are different (excited) from the self-consistent solutions due to the stochastic distribution. In the LVL calculation which started with the initial distribution of test particles having a sharp surface, test particles diffused and the local density [Eq. (66)] at the surface became similar to the solid line in Fig. 1 even before 10 fm/c (see Fig. 4 of Ref. 5). If we implemented the classical condition, Eq. (8), exactly and the numerical calculation was exact, the sharp surface should be maintained in the LVL calculation.

The local averaged densities are shown in Fig. 1 (solid lines) for each case. These densities are averaged over a time period of 30–180 fm/c. Since our initial distributions are not exact self-consistent ground states of a static nucleus due to the stochastic prescription and due to the fact that we have used $\delta(\mathbf{p}-\mathbf{p}_i)$ in Eq. (64) with $\mathbf{p}_i$ distributed randomly in a local Fermi sphere, there are some excited oscillation modes in the propagation of the system. Relaxing the density matrix condition to satisfy only Pauli condition also introduces an oscillation mode similarly as in going from TDHF to RPA or to extended TDHF. These oscillation modes are removed through the time average. As we can see in Fig. 1, the nuclear density at the surface region is much closer to the Hartree-Fock density than to the classical Vlasov solution for all the four cases independently of the initial distribution. Notice here that the slope at the surface region depends on the underlying force (the left column of Fig. 1 for the local force and the right column for the Yukawa force), but not on the initial distribution (similarity between LVL and LHF and between YVL and YHF). Specifically, for the YHF case, this calculation reproduced the Hartree-Fock density quite well over a whole nucleus except for the small ripples at the central region. There are some spatial oscillations in the central region of Hartree-Fock densities due to the shell effects in contrast to the classical Vlasov solutions (see Fig. 1). Since we have used the local averaged density over a sphere of radius $b\approx 1.2$ fm instead of the actual local density in the force calculation of Eq. (65), we cannot have these detailed oscillations in our calculation. Due to this diminishing effect of average density, the shell structure, which is a quantum effect, cannot be reproduced in our calculation. The local force cases, which have a larger shell structure at the central region than the Yukawa force, have a larger discrepancy from the HF self-consistent central densities and this caused some discrepancy for the surface density as well. If we kill the shell structure through the average in the local Hartree-Fock density, the central density would become constant for the local force. The central density is about constant in the LHF calculation (solid line) which started with the initial density having large oscillations in the central density (dashed line). If we choose a form factor for the test particles better than the point particle and use actual local

density instead of local averaged density[12] for the force calculation of Eq. (54), we would have oscillations in the central density through the test particle method. Even with point test particles using local averaged density, some of the quantum effects in the density appears. Figure 1 shows that the test particle method, Eqs. (46) and (47), reproduces the nuclear density much closer to TDHF than to the Vlasov equation which is a classical limit of TDHF.

Once we have the distribution of test particles in a nucleus at any time, we can calculate physical quantities. For the form factor of Eq. (64), the root-mean-square radius of a nucleus in configuration space $R_{\rm rms}$ and in momentum space $P_{\rm rms}$ become

$$R_{\rm rms}^2=\frac{1}{A}\int d^3rr^2\rho(\mathbf{r})=\frac{1}{N}\sum_{i=1}^{N} r_i^2 , \tag{68}$$

$$P_{\rm rms}^2=\frac{1}{A}\int d^3pp^2g(\mathbf{p})=\frac{1}{N}\sum_{i=1}^{N} p_i^2 , \tag{69}$$

where $g(\mathbf{p})$ is the nucleon distribution in momentum space, i.e., Eq. (22). From the time dependence of these two quantities, we can extract information about a monopole oscillation mode of the nucleus. Since a monopole mode is the radial vibration of a nucleus, the time dependence of

$$\langle R\cdot P\rangle=\frac{1}{A}\int d^3rd^3p[\mathbf{r}\cdot\mathbf{p}]f(\mathbf{r},\mathbf{p})=\frac{1}{N}\sum_{i=1}^{N}[\mathbf{r}_i\cdot\mathbf{p}_i] \tag{70}$$

also represents the monopole mode. Here Eqs. (29), (32), and (64) are used. These are shown in Fig. 2 for the LHF case on the left column and for the YHF case on the right column. The oscillation period T is about 45 fm/c for the local force (LHF) and about 50 fm/c for the Yukawa force (YHF). These correspond to the monopole oscillation energy ($\hbar\omega=2\pi\hbar/T$) of 27 MeV for the local force and 25 MeV for the Yukawa force; this is in good agreement with the empirical formula[9]

$$E(0^+)\approx 82A^{-1/3}\,\text{MeV}=24\text{MeV} .$$

A self-consistent calculation in a classical Vlasov equation[14] gives monopole oscillation energy of about 32 MeV for the Yukawa force which is too high. The empirical monopole energy also is reproduced by the test particle method.

We can also study the quadrupole oscillation mode. The quadrupole moments Q_{zz} of a nucleus in the configuration space and in the momentum space are, for point test particles,

$$Q_r=2\sqrt{4\pi/5}\int d^3rr^2Y_2^0(\theta,\phi)\rho(\mathbf{r})$$

$$=\int d^3r(3z^2-r^2)\rho(\mathbf{r})=\sum_{i=1}^{N}(2z_i^2-x_i^2-y_i^2) , \tag{71}$$

$$Q_p=\int d^3p(3p_z^2-p^2)g(\mathbf{p})=\sum_{i=1}^{N}(2p_{iz}^2-p_{ix}^2-p_{iy}^2) . \tag{72}$$

These are shown in Fig. 3 for LHF on the left column and for YHF on the right column. There is a phase shift of π between $Q_r(t)$ and $Q_p(t)$. This phase shift and nonzero Q_p indicate that there is a quadrupole deformation in the local Fermi sea for the quadrupole oscillation of a nucleus. The quadrupole oscillation period T is about 70 fm/c for the local force and about 75 fm/c for the Yukawa force. These give the quadrupole oscillation energy of 18 MeV for the local force and 17 MeV for the Yukawa force which are again in good agreement with the empirical formula $E(2^+)\approx 60A^{-1/3}\,\text{MeV}=17.5$ MeV.[9] Neglecting the quadrupole deformation of the Fermi sea, the self-consistent calculation in a classical Vlasov equation gives a very low quadrupole oscillation energy (about 6 MeV for the Yukawa force).[14] The quadrupole oscillation mode is also well reproduced through

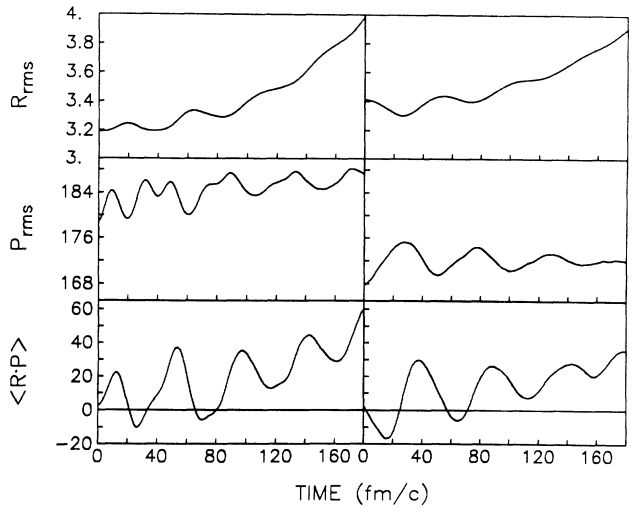

FIG. 2. Monopole oscillation mode in the test particle method. $R_{\rm rms}$ is in units of fm, $P_{\rm rms}$ is in units of MeV/c, and $\langle R\cdot P\rangle$ in units of fm×MeV/c. These are defined by Eqs. (68)–(70). The left column is for the local force and the right column is for the Yukawa force. The initial densities are Hartree-Fock densities (LHF and YHF) for the corresponding forces.

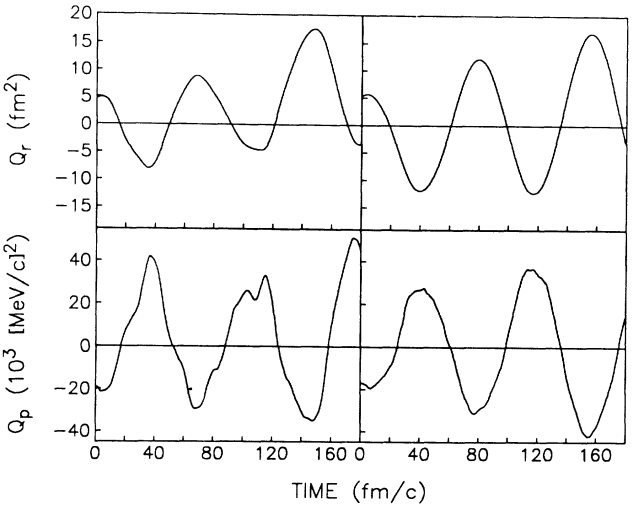

FIG. 3. Quadrupole oscillation mode for the same calculations as in Fig. 2. Q_r and Q_p are defined by Eqs. (71) and (72). The left column is for the local force (LHF) and the right column is for the Yukawa force (YHF).

the test particle method of Sec. III.

In Figs. 2 and 3, we can see that the monopole and quadrupole oscillations are not simple harmonic oscillations. To study the structure of this oscillation in detail, we consider the Fourier transform

$$A(\omega)=\int_0^{t_m} dt\, e^{-i\omega t}G(t)\ ,$$
$$I(\omega)=|A(\omega)|^2\ , \tag{73}$$

where $G(t)$ represents any of the time-dependent monopole or quadrupole moment. The time t_m should be large enough to include at least few period T of the oscillation. Thus, for this Fourier analysis, the system has been propagated up to $t_m=750$ fm/c. For Fourier analysis, we also considered octupole moments defined as

$$O_r=2\sqrt{4\pi/7}\int d^3r r^3 Y_3^0(\theta,\phi)\rho(\mathbf{r})$$
$$=\int d^3r z(5z^2-3r^2)\rho(\mathbf{r})=\sum_{i=1}^{N} z_i(2z_i^2-3x_i^2-3y_i^2)\ , \tag{74}$$

$$O_p=\int d^3p p_z(5p_z^2-3p^2)g(\mathbf{p})=\sum_{i=1}^{N} p_{iz}(2p_{iz}^2-3p_{ix}^2-3p_{iy}^2)\ . \tag{75}$$

The time dependencies of multipole moments in r and p space for YHF are shown on the left columns in Figs. 4 and 5, respectively. These are from the extended evolution up to $t_m=750$ fm/c of the system used for Figs. 2 and 3. The right columns are the same calculation (YHF) as the left columns except the test particles have different initial momentum at $t=0$ through different randomization which has positive $Q_p(t=0)$ in contrast to negative $Q_p(t=0)$ for the left column case (see Fig. 5). This new initialization also shows a phase shift of π between $Q_r(t)$ and $Q_p(t)$ (Figs. 4 and 5). The nucleus is quite stable up to $t=200$ fm/c but, after that, it is growing in r space (see Fig. 4) due to energy nonconservation originating from numerical inaccuracy. However, the system is quite stable up to $t=750$ fm/c in p space as we can see in Fig. 5, except $P_{\rm rms}$ which has a quite stable oscillation mode defined as

$$M_p(t)=P_{\rm rms}(t)-P_0+P_2\left[\frac{t}{t_m}\right]^2\ . \tag{76}$$

In Fig. 5, M_p+P_0 are shown (dotted lines) with $P_0=172.2$ MeV/c for the left column and $P_0=172.7$ MeV/c for the right column; $P_2=10.9$ MeV/c and $t_m=750$ fm/c. The intensity $I(\omega)$ for the Fourier transform, Eq. (73), of $M_p(t)$ (first row), $Q_p(t)$ (second row), and $O_p(t)$ (last row) are shown in Fig. 6. Figure 6 illustrates the rich structure of vibration modes which is similar to the extended TDHF with TDDM.[3] The details of the spectrum depend on the initial distribution, differences between the left and the right columns in Fig. 6. However, both initializations show quite similar peak

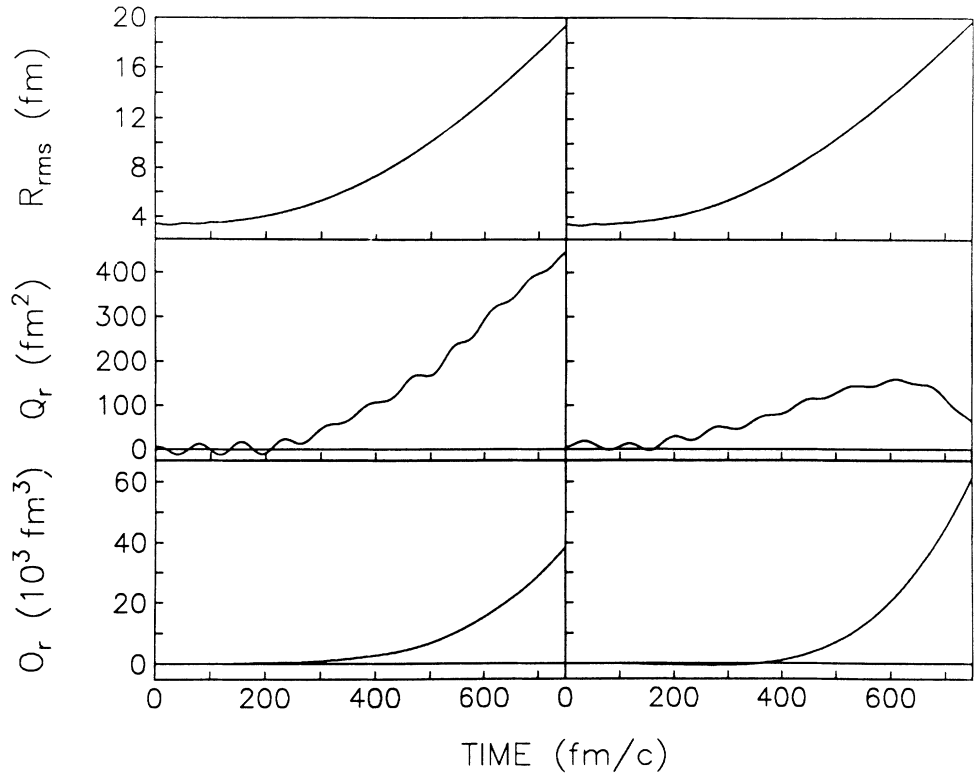

FIG. 4. Time dependence of monopole ($R_{\rm rms}$), quadrupole (Q_r), and octupole (O_r) modes in r space. The left column is for YHF and the right column is the same as YHF but with different initial momentum distribution.

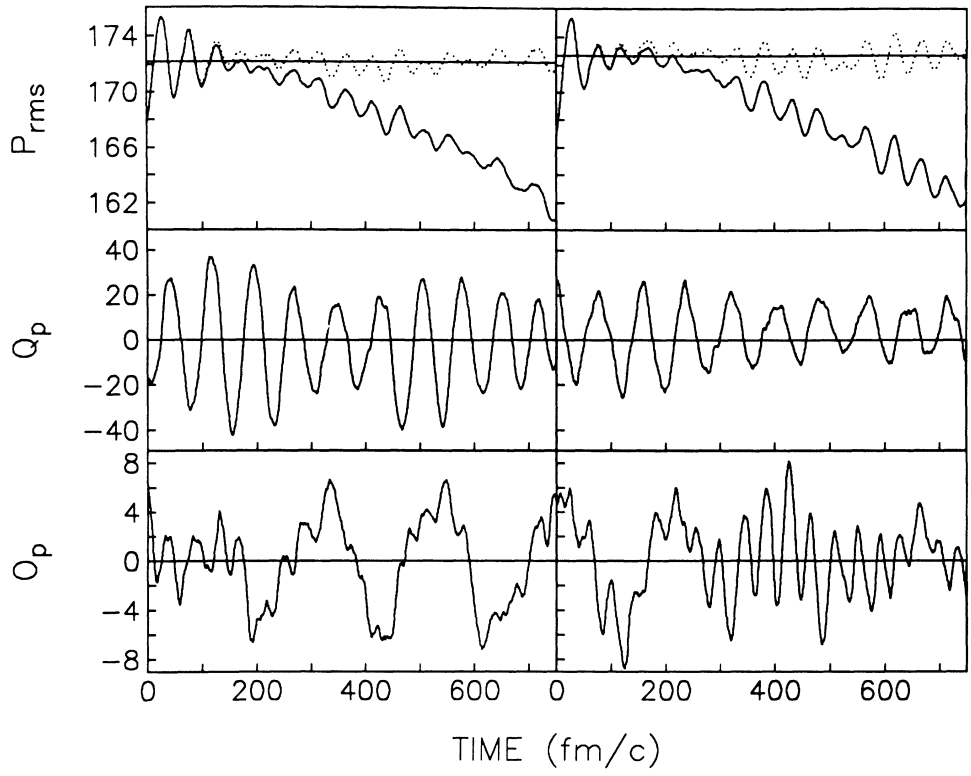

FIG. 5. Same as in Fig. 4 but in p space. The dotted lines in the first row are the corresponding M_p+P_0 of Eq. (76). $P_{\rm rms}$ is in the unit of MeV/c, Q_p in 10^3 (MeV/c)^2, and O_p in 10^6 (MeV/c)^3.

positions. The monopole mode peaked at about 25 MeV and the quadrupole mode at about 16 MeV as seen from Figs. 2 and 3. There clearly are two peaks in the octupole mode; one at about 6 MeV and one at about 30 MeV. These are in good agreement with the empirical formula $53A^{-2/3}\,\mathrm{MeV}=4.5\mathrm{MeV}$,[15] for the low lying octupole mode, and $108A^{-1/3}\,\mathrm{MeV}=31.6$ MeV,[16] for the giant octupole resonance. A self-consistent calculation in a classical Vlasov equation[14] gives an octupole oscillation energy of 12 MeV for the Yukawa force which corresponds to the surface vibration in a liquid drop model.[17] A classical Vlasov equation for a spherical harmonic oscillator with a separable octupole-octupole force without self-consistency does not give a low-lying octupole mode[8]. The octupole oscillation modes are also well reproduced by the test particle method.

Fourier analysis (Fig. 6) shows that the test particle method reproduces multipole modes very similar to quantal RPA (Ref. 9) or TDDM (Ref. 3) calculations rather than to TDHF itself. In practical calculations of the test particle method, the density matrix condition [Eqs. (14) or (8)] is relaxed to Eq. (50) similarly as in the RPA or TDDM. However, there is no clear way to control this relaxation $(\rho^2-\rho)$ in contrast to the RPA or TDDM case. Two-body collisions are responsible for this relaxation in TDDM and Eq. (2) is satisfied up to first order of $\delta\rho=\rho-\rho_0$ in RPA. Response calculations using the Vlasov equation with a self-consistent residual interaction[18] also produce similar results for vibration modes. $\rho^2-\rho$ is nonzero in this calculation[18,19] as in RPA which corresponds to a small amplitude approximation of TDHF. Except for the classical solutions of Ref. 14 which explicitly satisfy Eq. (8), all other calculations using a self-consistent residual interaction compared here, produce similar resonance energies which are close to empirical values. However, without the m^*/m correction, the test particle method gives a dipole resonance energy which is too low.[20]

V. SUMMARY AND CONCLUSION

Quantum extension of the Vlasov equation has been established using the test particle method to the full Wigner transform of TDHF without truncation in $\hbar$ order. Decomposing the Wigner function in terms of test particles with the form factor in a phase space, quantum extension of the Vlasov equation [Eq. (12)] provides the equation of motion [Eq. (33)] for the test particles. Integrating Eq. (33) over p or r space, which are the special cases of inverse Wigner transform, we get the quantum description for the equation of motion of test particles, Eqs. (36) and (37). Integrating these equations over r or p space, respectively, which correspond to taking the expectation value, we get coupled equations of motion [Eqs. (38) and (39)] for the test particles. Notice here that these equations are necessary but not sufficient conditions of

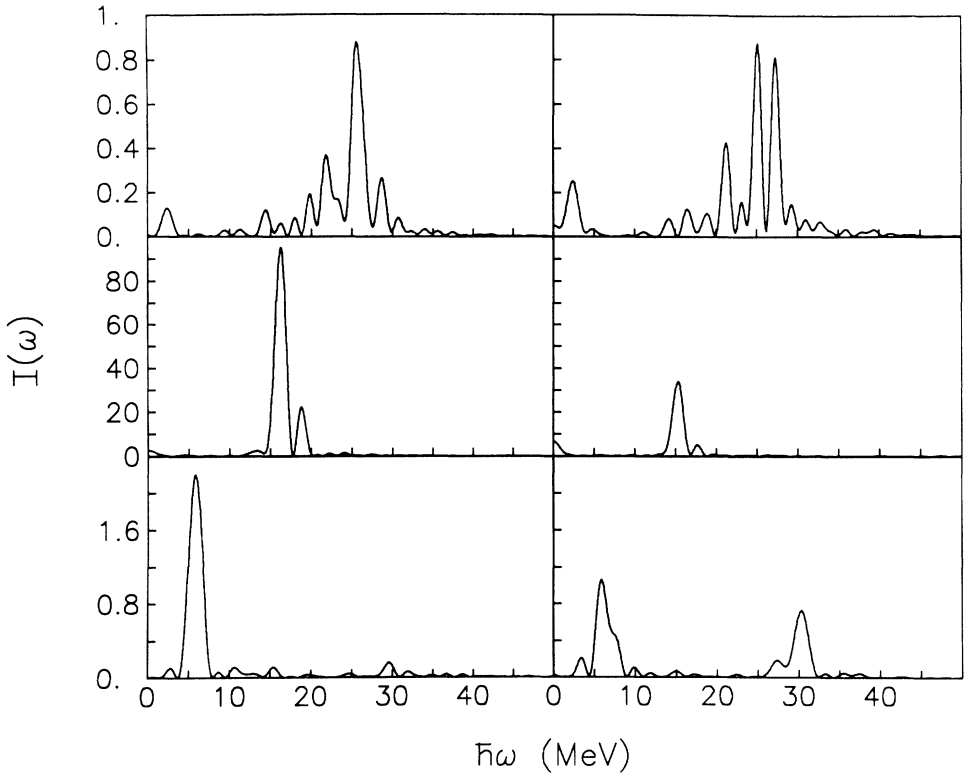

FIG. 6. The intensities $I(\omega)$ of the Fourier transform, Eq. (73), of the corresponding multipole vibration modes in p space (Fig. 5). The first row is for M_p in units of 10^{-1} $[(\mathrm{MeV}/c)(\mathrm{fm}/c)]^2$, the second row is for Q_p in $[10^3(\mathrm{MeV}/c)^2\,(\mathrm{fm}/c)]^2$, and the last row is for O_p in $[10^6(\mathrm{MeV}/c)^3(\mathrm{fm}/c)]^2$.

Eqs. (36) and (37). The sufficient but not necessary conditions of Eqs. (38) and (39) give the equations of motion [Eqs. (46) and (47)] for each test particle which follow classical dynamics with averaged force and velocity of the test particle. These equations are exactly the same as the equations of motion for the test particle used in BUU calculations with the classical Vlasov equation.[4,7]

The discrimination between quantum and classical description is related with the constraint on the density matrix, namely Eq. (14) for the quantum case and Eq. (8) for the classical case. Since imposing these conditions in the test particle method is very hard, these have been relaxed to satisfy only the Pauli principle represented by Eq. (50). The condition (14) is more restrictive than the condition (50) and less restrictive than the classical condition (8). Therefore, without explicit use of the condition of Eq. (8), the test particle method becomes the quantum description of a system, naturally. Furthermore, the relaxation of the density matrix condition makes the test particle method become more like some extensions of TDHF, which involve more than one Slater determinant, instead of TDHF itself. The details of the solution depend on what conditions are actually satisfied by the Wigner function. This is the actual reason why we have quantum effects (such as diffuse surface) in the test particle method, not because of using Gaussians for the form factor as claimed in Ref. 7. Using Gaussians may give a better answer because we can use a more accurate numerical procedure but not because of any special characteristics of Gaussians.

Through numerical calculations using the simplest form factor of Eq. (64) (point particle) for the test particles, we have shown that the test particle method actually reveals quantum effects in the nuclear density distribution and even in the multipole vibration modes. Due to the numerical error related with using point test particles, we have studied limited observables only. Since Eqs. (38) and (39) are not the sufficient conditions of Eqs. (36) and (37), there are some extra missing conditions to be satisfied by test particles. Furthermore, we have only shown that Eqs. (46) and (47) are sufficient conditions to be satisfied by each test particle without any consideration of necessary conditions. There is no clear way to control the amount of violation of the density matrix condition $(\rho^2-\rho)$. If we can implement the density matrix condition Eqs. (14) or (8) exactly, then the test particle method becomes equivalent to the TDHF or the semiclassical Vlasov calculations, respectively. These points should be investigated further.

ACKNOWLEDGMENTS

Discussions with S. Das Gupta and N. de Takacsy are gratefully acknowledged. This work was supported in part by the National Sciences and Engineering Research Council and in part by the Quebec Department of Education.

*Present address: Department of Physics and Astronomy, Rutgers University, Piscataway, NJ 08855.

[1]M. Tohyama, Phys. Rev. C **36**, 187 (1987).
[2]M. Tohyama and M. Gong, Michigan State University Report MSUCL-657, 1988.
[3]M. Gong and M. Tohyama, Michigan State University Report MSUCL-656, 1988; M. Tohyama, Phys. Rev. C **38**, 553 (1988).
[4]G. F. Bertsch and S. Das Gupta, Phys. Rep. **160**, No. 4 (1988).
[5]S. J. Lee, H. H. Gan, E. D. Cooper, and S. Das Gupta, Phys. Rev. C **40**, 2585 (1989).
[6]S. J. Lee and S. Das Gupta (unpublished).
[7]C. Gregoire, B. Remaud, F. Sebille, L. Vinet, and Y. Raffray, Nucl. Phys. **A465**, 317 (1987).
[8]H. Kohl, P. Schuck, and S. Stringari, Nucl. Phys. **A459**, 265 (1986).
[9]P. Ring and P. Schuck, *The Nuclear Many-Body Problem* (Springer-Verlag, New York, 1980).
[10]S. Das Gupta, C. Gale, J. Gallego, H. H. Gan, and R. D. Ratna Raju, Phys. Rev. C **35**, 556 (1987).
[11]P. Schuck *et al.*, Prog. Part. Nucl. Phys. **22**, 181 (1989).
[12]R. J. Lenk and V. R. Pandharipande, Phys. Rev. C **39**, 2242 (1989).
[13]S. J. Lee, A. S. Umar, K. T. R. Davies, M. R. Strayer, and P.-G. Reinhard, Phys. Lett. B **196**, 419 (1987).
[14]S. J. Lee, E. D. Cooper, H. H. Gan, and S. Das Gupta, Phys. Rev. C **41**, 706 (1990).
[15]S. Stringari, Phys. Lett. **103B**, 5 (1981).
[16]F. E. Bertrand, in *Studying Nuclei with Medium Energy Protons,* University of Alberta/TRIUMF Workshop, July 1983, edited by J. M. Greben (TRIUMF, Vancouver, 1983), p. 181.
[17]A. Bohr and B. Mottelson, *Nuclear Structure* (Benjamin, New York, 1969), Vol. II.
[18]G. F. Burgio and M. Di Toro, Nucl. Phys. B **476**, 189 (1988).
[19]D. M. Brink, A. Dellafiore, and M. Di Toro, Nucl. Phys. **A456**, 205 (1986).
[20]E. Suraud, M. Pi, and P. Schuck, Nucl. Phys. **A482**, 187c (1988).